Wavelength-by-wavelength temperature-independent thermal radiation utilizing an insulator–metal transition

Jonathan King[1*], Alireza Shahsafi[1*], Zhen Zhang[3], Chenghao Wan[1,2], Yuzhe Xiao[1], Chengzi Huang[3], Yifei Sun[3], Patrick J. Roney[1], Shriram Ramanathan[3] and Mikhail A. Kats[1,2,4]

[1]Department of Electrical and Computer Engineering, University of Wisconsin-Madison

[2]Department of Materials Science and Engineering, University of Wisconsin-Madison

[3]School of Materials Engineering, Purdue University, West Lafayette, Indiana

[4]Department of Physics, University of Wisconsin-Madison

[*]Authors contributed equally

Abstract

Both the magnitude and spectrum of the blackbody-radiation distribution change with temperature. Here, we designed the temperature-dependent spectral emissivity of a coating to counteract all the changes in the blackbody-radiation distribution over a certain temperature range, enabled by the nonhysteretic insulator-to-metal phase transition of $SmNiO_3$. At each wavelength within the long-wave infrared atmospheric-transparency window, the thermal radiance of our coating remains nearly constant over a temperature range of at least 20 °C. Our approach can conceal thermal gradients and transient temperature changes from infrared imaging systems, including those that discriminate by wavelength, such as multispectral and hyperspectral cameras.

The imaging of thermal radiation using infrared cameras forms the basis of night vision, and enables the measurement of temperature profiles on the surfaces of remote objects. As such, the obfuscation of temperature information provided by infrared imaging is an ongoing research area, with approaches being explored that manipulate one or more of surface temperature, emissivity, and scattering. Active control of temperature [1] or emissivity [2]–[5] can dynamically alter thermal signatures using external power and control circuitry, which in the best case can render an object invisible to an infrared camera by displaying an infrared image of what is behind the object. Passive systems that do not require external power typically cannot dynamically reproduce infrared images that are behind an object, but they can provide a variety of

other capabilities. These passive systems include scattering and absorbing screens that block radiation from an object and equilibrate with the environment, and thus can mimic ambient radiation [6]; enclosures with position-dependent effective thermal conductance that enables the replication of a background temperature distribution onto the enclosure exterior [7]; and coatings with non-trivial temperature-dependent emissivities that can make the emitted thermal radiation of an object not depend on temperature [8]. This last class of infrared-concealment systems—passive coatings based on temperature-dependent emissivity—is the focus of this paper.

Such coatings require the incorporation of materials whose infrared properties change strongly with relatively small changes in temperature. For this purpose, phase-transition materials such as vanadium dioxide (VO_2) [9], germanium-antimony-tellurium (GST) [10][11], and samarium nickel oxide ($SmNiO_3$) [8] have been explored. Phase-transition materials have been leveraged to enable dynamic thermal emission for a variety of applications including smart windows [12], satellite thermal regulation [13]–[15], and passive daytime cooling [16], in addition to thermal camouflage [2][3].

Among the materials that have been explored for thermal-emission engineering, $SmNiO_3$ is a newcomer, but its unique combination of characteristics provides functionality not found in other material systems. The optical properties of $SmNiO_3$ films can exhibit a strong and steady evolution over tens of degrees (from 25 °C to 140 °C [8]), with especially large changes in the mid- and long-wave infrared, i.e., the wavelength ranges commonly used by infrared imaging systems. Unlike other materials with insulator-to-metal transitions (IMTs), thin films of $SmNiO_3$ can be synthesized such that the hysteresis often associated with IMTs appears to be negligible or absent [17][18].

In 2019, our groups demonstrated the use of $SmNiO_3$ films to realize "zero-differential thermal emitters", or ZDTEs, in which the thermal emission from a coating has a roughly constant power with respect to temperature, when integrated over the wavelength range of the long-wave infrared atmospheric transparency window (8–14 μm) [8]. ZDTEs can be used to conceal information typically present in heat signatures picked up by off-the-shelf infrared cameras. However, in these ZDTEs, only the wavelength-integrated radiated power remains constant with temperature, and the films cease to appear zero-differential when imaged using a hyperspectral camera or even bandpass filters positioned in front of a conventional infrared camera[1].

Here, we designed and demonstrated "zero-differential spectral emitters" (ZDSEs), which are passive emission coatings that feature temperature-independent spectral radiance, and can thus conceal information

[1] We note that existing active infrared camouflage systems that are designed to display infrared images of what is behind an object have a similar limitation to our ZDTEs in that they modulate the emitted power rather than the full emitted spectrum.

even from hyperspectral infrared cameras that discriminate by wavelength. In other words, we designed the temperature-dependent emissivity of a coating to counteract the intrinsic temperature-dependent changes at each wavelength in the blackbody thermal-emission spectrum.

Design and optimization

Any object emits thermal radiation, with the emitted temperature-dependent spectral radiance given by [19]

$$I(\lambda, T) = \varepsilon(\lambda, T) I_{BB}(\lambda, T) \qquad (1),$$

where $\varepsilon(\lambda, T)$ is the object's spectral emissivity and $I_{BB}(\lambda, T)$ is the spectral radiance of a blackbody, which is given by Planck's law [20] [Fig. 1(a)]:

$$I_{BB}(\lambda, T) = \frac{2hc^2}{\lambda^5} \frac{1}{e^{\frac{hc}{\lambda k_B T}} - 1}. \qquad (2)$$

Here, h is Planck's constant, k_B is Boltzmann's constant, c is the free-space speed of light, λ is free-space wavelength, and T is the absolute temperature.

To achieve temperature-independent spectral radiance, we require $dI(\lambda, T)/dT = 0$ for every wavelength of interest. The solution to this differential equation requires the emissivity to be in the form (*SI Appendix*, section 1)

$$\varepsilon(\lambda, T) = f(\lambda)\left(e^{\frac{hc}{\lambda k_B T}} - 1\right), \qquad (3)$$

where $f(\lambda)$ is any function of λ. Eqn. (3) provides a substantial degree of freedom when designing coatings with temperature-independent spectral radiance, since $f(\lambda)$ is an arbitrary function [Fig. 1(b)].

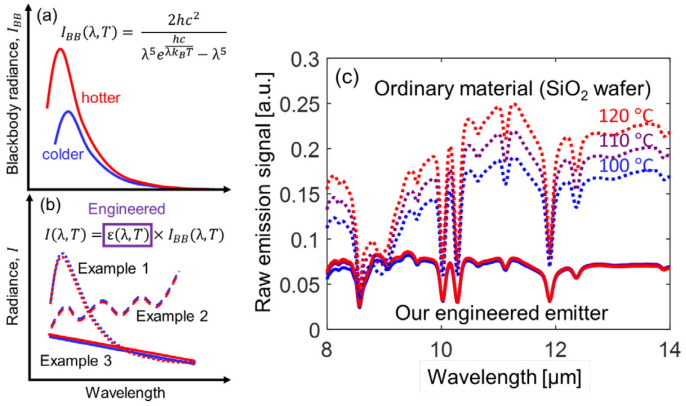

Figure 1) (a) Blackbody spectral radiance, $I_{BB}(\lambda, T)$, at two arbitrary temperatures. **(b)** Several examples of temperature-dependent spectral radiance where $dI(\lambda, T)/dT = 0$ is achieved by engineering the emissivity. (c) The main experimental result of this paper: an emitter engineered to achieve $dI(\lambda, T)/dT = 0$ across the 8 – 14 μm from T

= 100 °C to T = 120 °C compared to a reference SiO_2 wafer (the sharp features are due to absorption by ambient gases present in the lab on the day of the measurement).

Our goal was therefore to implement a form of $\varepsilon(\lambda, T)$ that satisfied Eqn. (3) over the long-wave atmospheric transparency range (8 to 14 μm) using $SmNiO_3$. We hypothesized that the design process would be simpler if the substrate for the $SmNiO_3$ film was reflective and did not have any abrupt features in its spectrum in the 8 – 14 μm range. Indium tin oxide (ITO) is well-suited for this purpose, which depending on its stoichiometry can be reflective and featureless in our wavelength range of interest [21].

Based on this argument, we selected our structure to be a thin-film assembly of $SmNiO_3$, ITO, and a substrate [Fig. 2(a)], with the thicknesses of the films (d_{SNO} for $SmNiO_3$ and d_{ITO} for ITO) to be determined by an optimization process. We chose the substrate to be soda-lime glass due to the commercial availability of inexpensive ITO films on these substrates.

To find the ideal thicknesses of the layers of the $SmNiO_3$ and ITO films, we used the transfer-matrix method to calculate the reflectance for different layer thicknesses, which we converted to emissivity using Kirchhoff's law, and then combined with Planck's law to determine the emitted spectral radiance (Fig. 2). We selected a figure of merit (to be minimized) that reasonably captures how close an emitter is to a ZDSE around a given temperature T:

$$\Phi(T) = \int_{\lambda_1}^{\lambda_2} 1/I(\lambda, T) \cdot |\partial I(\lambda, T)/\partial T| \, d\lambda \qquad (4)$$

Note that a simpler figure of merit that omits the $1/I(\lambda, T)$ term in Eqn. (4) can also be used to find solutions with small absolute changes of radiance with temperature, but these solutions would often simply be "trivial" low-emissivity designs; note that an object with $\varepsilon(\lambda, T) = 0$ is always zero-differential. Instead, the full Eqn. (4) can be used to find nontrivial ZDSE designs with emissivity values much greater than 0.

In these calculations, we used the refractive indices of $SmNiO_3$ that we measured previously [8] [Fig. 2(b) and Fig. 2(c)]. The refractive indices of ITO were derived from Drude-theory calculations, assuming a free-carrier density of $n_e = 8 \times 10^{20}$ cm^{-3} (see calculations with other n_e values in *SI*, section 3). Because soda-lime glass is mostly SiO_2 and we expected most light not to reach the substrate anyway, we used the complex refractive index of SiO_2 glass [22] to describe the soda-lime substrate in the calculations. We chose to perform our ZDSE optimization around 110 °C based on the location of the phase transition and availability of refractive-index data.

The resulting map of the figure of merit $\Phi(T = 110\ °C)$ is shown in Fig. 2(d). The device achieves good performance (i.e., minimal $\Phi(T = 110\ °C)$) at d_{SNO} > 200 nm and almost any value of d_{ITO}, though d_{ITO} can be used as a fine-tuning knob to slightly change Φ. The optimal parameters were $d_{SNO} \sim$ 320 nm and

d_{ITO} ~ 500 nm. Note that the minima in Fig. 2(d) are broad, so for ease of fabrication, we chose a slightly suboptimal set of parameters, with a thinner film of $SmNiO_3$, to make it easier to deposit [Fig. 2(d)].

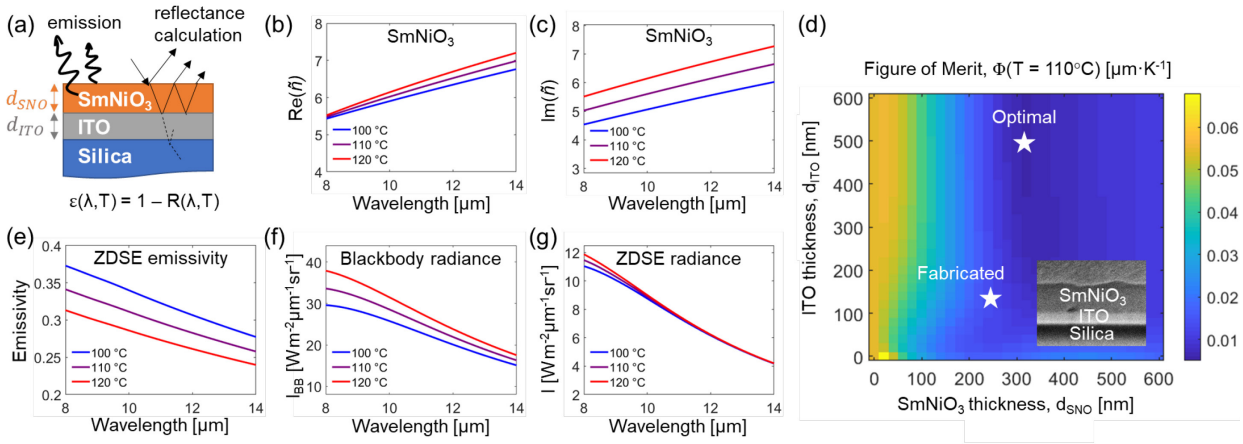

Figure 2) (a) Thin-film assembly consisting of $SmNiO_3$ and ITO films on top of a soda-lime glass substrate (assumed to be pure silica in the simulations). Spectral emissivity is calculated as $1 - R(\lambda, T)$ using the transfer-matrix method. **(b)** Real and **(c)** imaginary parts of the complex refractive index of the $SmNiO_3$ film from T = 100 °C to T = 120 °C [8], which served as an input for our transfer-matrix calculations. The indices at T = 110 °C were interpolated from data at T = 100 °C and T = 120 °C. **(d)** Calculated optimization space based on the integrated normalized absolute rate change of spectral radiance with respect to temperature [figure of merit, $\Phi(T)$]. The optimal structure dimensions and actual dimensions of our fabricated device are marked by white stars. The inset is an SEM cross-section of the fabricated structure. **(e)** Spectral emissivity of the optimal zero-differential spectral emitter (ZDSE) from T = 100 °C to T = 120 °C for 8 μm < λ < 14 μm. **(f)** Spectral radiance of a blackbody from T = 100 °C to T = 120 °C. **(g)** Spectral radiance of the optimal ZDSE with $SmNiO_3$ and ITO thicknesses of 320 and 500 nm, respectively. Radiance is calculated by multiplying the spectral emissivity by blackbody spectral radiance for each temperature.

Fabrication and experiments

We fabricated a sample having dimensions that were within the high-performance design space [dark blue region in Fig. 2(g)]. The thicknesses of $SmNiO_3$ and ITO were $d_{SNO} = 234 \pm 18$ nm and $d_{ITO} = 120 \pm 5$ nm, respectively, measured after fabrication using scanning electron microscopy (SEM) cross section images (details and images provided in *SI Appendix*, section 4). Our ITO-coated soda-lime glass substrate was purchased from Sigma Aldrich, and had a resistivity of 8-12 Ω/sq. $SmNiO_3$ thin films were magnetron co-sputtered from Ni and Sm targets at room temperature. DC power of 90 W was applied to Ni target, and RF power of 170 W was applied to Sm target. The stoichiometric ratio of Sm and Ni was calibrated with energy dispersive spectroscopy. During deposition, the pressure of the chamber was kept at 5 mTorr with flow of Ar (40 sccm) and O_2 (10 sccm) gases. To form the perovskite phase, the as-grown films were annealed at 500 °C in pure oxygen gas at 1400 psi for 24 hours.

The reflectance of our fabricated ZDSE was measured using Fourier-transform spectroscopy (FTS, Hyperion 2000 microscope coupled to Bruker Vertex 70 spectrometer) and a temperature-controlled heat stage, as shown in Fig. 3(a), and the emissivity was obtained via Kirchhoff's law for opaque, non-scattering samples (*i.e.*, $\varepsilon = 1 - R$) [8]. The emissivity of the fabricated ZDSE [Fig. 3(a)] roughly resembles our optimized theoretical emissivity shown in Fig. 2(e), thus approaching the intended spectral and thermal dependencies that satisfy the criterion of $dI(\lambda, T)/dT = 0$. As a result, the figure of merit [Eqn. (4)] of our fabricated ZDSE is $\Phi(T) \sim 0.007$ μm·K^{-1}, which is close to the theoretical minimum of $\Phi(T) \sim 0.006$ μm·K^{-1}. The nearly temperature-independent spectral radiance was observed directly by measuring the raw emission signal of the heated sample using our FTS setup described previously [23], as shown in Fig. 3(b). The same sample was also measured on another day, and directly compared to a reference SiO_2 wafer [Fig. 1(c)], demonstrating its broad temperature-independence at each wavelength within the long-wave infrared.

We also imaged the samples using a long-wave infrared camera (FLIR A325sc) with and without spectral filters between the camera and the sample, to demonstrate temperature independence in various spectral bands. When performing infrared imaging with this type of camera, typically the user inputs a wavelength-averaged emissivity ε_{set}, as well as measurement conditions such as the background temperature, and the camera software then reports a temperature, which we refer to as the "apparent temperature". Because in our sample the actual emissivity changes with temperature, there is ambiguity about what ε_{set} should be. For Fig. 3(c), we first set our temperature stage to 90 °C, and varied ε_{set} until the apparent temperature of the sample was roughly 90 °C. We then maintained ε_{set} at the same value for measurements at elevated temperatures. These values of ε_{set} are reported in Fig. 3(c). Additional IR images and analysis are provided in *SI Appendix*, section 7.

Additional temperature-dependent reflection measurements with heating and cooling cycles were performed to confirm the non-hysteretic IMT in our $SmNiO_3$ film (*SI Appendix*, section 6). We note that the fabricated structure was not uniform, which is apparent from the infrared images in Fig. 3(c) as well as in additional FTS measurements that we provide in *SI Appendix*, section 5. In the infrared images, specks appear on the surface and become more distinct as temperature increases. The specks are likely defects in the $SmNiO_3$ film or dust particulates on the surface.

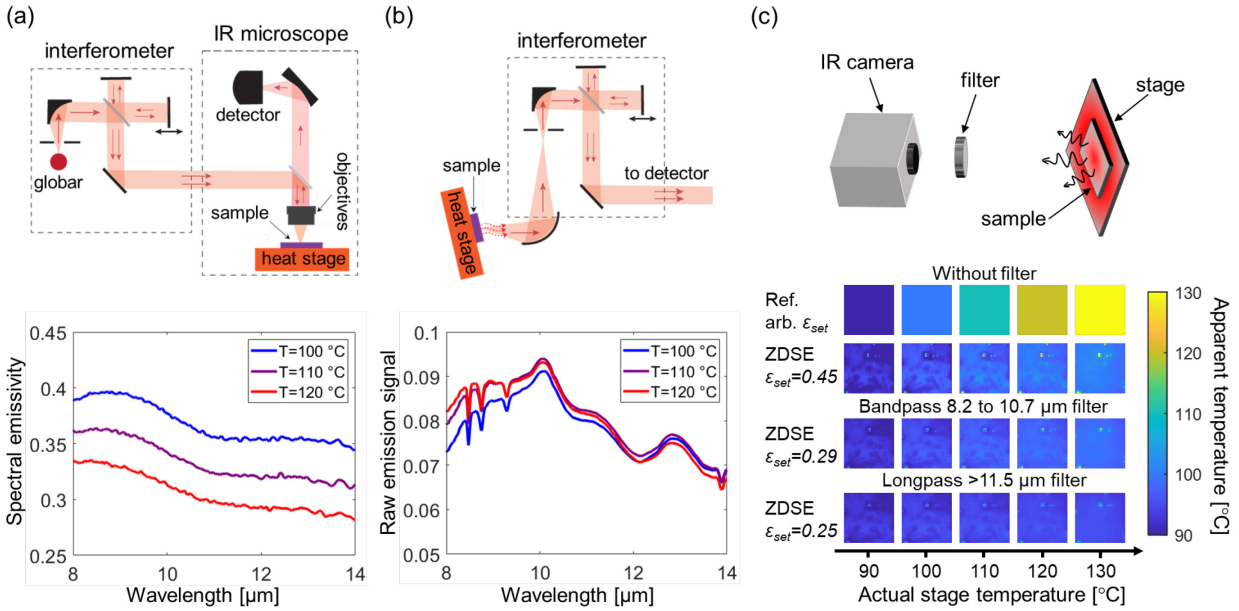

Figure 3) (a) (Top) Schematic of reflectance measurements used to obtain spectral emissivity values of our ZDSE and (bottom) resultant spectral emissivity from 100 to 120 °C. **(b)** (Top) Schematic of direct emission measurements and (bottom) the raw spectral emission signal of the ZDSE measured from 100 to 120 °C. The sharp features at 8 < λ < 10 μm are atmospheric absorption lines. **(c)** (Top) Infrared imaging setup and (bottom) infrared images of the ZDSE with and without spectral filters. The "apparent temperature" is the value reported by the FLIR infrared camera when the input emissivity ε_{set} was selected such that the apparent temperature matched the stage temperature at 90 °C (see main text for more details).

Discussion and conclusion

It is not trivial that a coating can be engineered to precisely cancel the changes in the Planck distribution for all individual wavelengths within a broad wavelength band (a "zero-differential spectral emitter", or ZDSE), over a broad range of temperatures. The emissivity spectra required for a ZDSE must satisfy Kramers-Kronig relations, while using combinations of materials with appropriate temperature-dependent optical properties and micro/nanostructure. However, since there are many solutions to Eqn. (3), we were able to find a practical solution based on the phase transition of samarium nickel oxide ($SmNiO_3$) for the long-wave infrared atmospheric transparency window.

We experimentally demonstrated a ZDSE based on films of $SmNiO_3$ and indium tin oxide (ITO), which achieves temperature-independent spectral radiance from ~90 to ~130 °C in the long-wave atmospheric transparency window of 8 to 14 μm. Future ZDSE designs may employ quaternary alloys such as $Sm_XNd_{1-X}NiO_3$, which can shift the phase transition to lower temperatures compared to $SmNiO_3$ [17], or vanadium dioxide (VO_2) where the intrinsic hysteresis of its phase transition can be minimized by doping [24][25].

The ZDSE conceals temperature gradients and transient temperature swings on a surface from infrared detection. More broadly, consideration of not only thermally emitted power but also the spectrum is required for any technology—passive or active—that aims to conceal infrared signatures from multispectral and hyperspectral imaging systems.

References

[1] S. Hong, S. Shin, and R. Chen, "An Adaptive and Wearable Thermal Camouflage Device," *Adv. Funct. Mater.*, vol. 30, no. 11, pp. 1–7, 2020, doi: 10.1002/adfm.201909788.

[2] Y. Qu *et al.*, "Thermal camouflage based on the phase-changing material GST," *Light Sci. Appl. 2018 71*, vol. 7, no. 1, pp. 1–10, Jun. 2018, doi: 10.1038/s41377-018-0038-5.

[3] Q. Kang, D. Li, K. Guo, J. Gao, and Z. Guo, "Tunable Thermal Camouflage Based on GST Plasmonic Metamaterial," *Nanomaterials*, vol. 11, no. 2, p. 260, Jan. 2021, doi: 10.3390/nano11020260.

[4] C. Xu, G. T. Stiubianu, and A. A. Gorodetsky, "Adaptive infrared-reflecting systems inspired by cephalopods," *Science (80-.).*, vol. 359, no. 6383, pp. 1495–1500, Mar. 2018, doi: 10.1126/science.aar5191.

[5] W. J. Padilla and X. Liu, "Reconfigurable room temperature metamaterial infrared emitter," *Opt. Vol. 4, Issue 4, pp. 430-433*, vol. 4, no. 4, pp. 430–433, Apr. 2017, doi: 10.1364/OPTICA.4.000430.

[6] M. J. Moghimi, G. Lin, and H. Jiang, "Broadband and Ultrathin Infrared Stealth Sheets," *Adv. Eng. Mater.*, vol. 20, no. 11, p. 1800038, Nov. 2018, doi: 10.1002/ADEM.201800038.

[7] Y. Li, X. Bai, T. Yang, H. Luo, and C. W. Qiu, "Structured thermal surface for radiative camouflage," *Nat. Commun. 2018 91*, vol. 9, no. 1, pp. 1–7, Jan. 2018, doi: 10.1038/s41467-017-02678-8.

[8] A. Shahsafi *et al.*, "Temperature-independent thermal radiation," *Proc. Natl. Acad. Sci. U. S. A.*, vol. 116, no. 52, pp. 26402–26406, Dec. 2019, doi: 10.1073/pnas.1911244116.

[9] C. Wan *et al.*, "On the Optical Properties of Thin-Film Vanadium Dioxide from the Visible to the Far Infrared," *Ann. Phys.*, vol. 531, no. 10, p. 1900188, Oct. 2019, doi: 10.1002/andp.201900188.

[10] Y. Zhang *et al.*, "Broadband transparent optical phase change materials for high-performance nonvolatile photonics," *Nat. Commun.*, vol. 10, no. 1, 2019, doi: 10.1038/s41467-019-12196-4.

[11] B. S. Lee, J. R. Abelson, S. G. Bishop, D. H. Kang, B. K. Cheong, and K. B. Kim, "Investigation of the optical and electronic properties of Ge 2Sb 2Te 5 phase change material in its amorphous, cubic, and hexagonal phases," *J. Appl. Phys.*, vol. 97, no. 9, p. 093509, Apr. 2005, doi: 10.1063/1.1884248.

[12] Y. Cui *et al.*, "Thermochromic VO2 for Energy-Efficient Smart Windows," *Joule*, vol. 2, no. 9. Cell Press, pp. 1707–1746, Sep. 19, 2018, doi: 10.1016/j.joule.2018.06.018.

[13] A. M. Morsy *et al.*, "Experimental demonstration of dynamic thermal regulation using vanadium dioxide thin films," *Sci. Rep.*, vol. 10, no. 1, pp. 1–10, Dec. 2020, doi: 10.1038/s41598-020-70931-0.

[14] K. Sun *et al.*, "VO2 Thermochromic Metamaterial-Based Smart Optical Solar Reflector," *ACS Photonics*, vol. 5, no. 6, pp. 2280–2286, 2018, doi: 10.1021/acsphotonics.8b00119.

[15] H. Kim *et al.*, "VO2-based switchable radiator for spacecraft thermal control," *Sci. Rep.*, vol. 9, no. 1, Dec. 2019, doi: 10.1038/s41598-019-47572-z.

[16] M. Ono, K. Chen, W. Li, and S. Fan, "Self-adaptive radiative cooling based on phase change materials," *Opt. Express*, vol. 26, no. 18, p. A777, 2018, doi: 10.1364/oe.26.00a777.

[17] S. Catalano, M. Gibert, J. Fowlie, J. Iñiguez, J. M. Triscone, and J. Kreisel, "Rare-earth nickelates RNiO3: Thin films and heterostructures," *Reports on Progress in Physics*, vol. 81, no. 4. Institute of Physics Publishing, p. 046501, Feb. 14, 2018, doi: 10.1088/1361-6633/aaa37a.

[18] S. Catalano *et al.*, "Electronic transitions in strained SmNiO3 thin films," *APL Mater.*, vol. 2, no. 11, Nov. 2014, doi: 10.1063/1.4902138.

[19] R. W. Boyd, *Radiometry and the detection of optical radiation*. 1983.

[20] M. Planck, "On the law of distribution of energy in the normal spectrum," *Ann. Phys.*, vol. 4, no. 553, p. 1, 1901.

[21] I. Hamberg and C. G. Granqvist, "Evaporated Sn-doped In2O3 films: Basic optical properties and applications to energy-efficient windows," *J. Appl. Phys.*, vol. 60, no. 11, 1986, doi: 10.1063/1.337534.

[22] J. Kischkat *et al.*, "Mid-infrared optical properties of thin films of aluminum oxide, titanium dioxide, silicon dioxide, aluminum nitride, and silicon nitride," *Appl. Opt.*, vol. 51, no. 28, pp. 6789–6798, 2012, doi: 10.1364/AO.51.006789.

[23] Y. Xiao *et al.*, "Precision Measurements of Temperature-Dependent and Nonequilibrium Thermal Emitters," *Laser Photon. Rev.*, vol. 14, no. 8, p. 1900443, Aug. 2020, doi: 10.1002/lpor.201900443.

[24] K. Miyazaki, K. Shibuya, M. Suzuki, K. Sakai, J. I. Fujita, and A. Sawa, "Chromium-niobium co-doped vanadium dioxide films: Large temperature coefficient of resistance and practically no thermal hysteresis of the metal-insulator transition," *AIP Adv.*, vol. 6, no. 5, 2016, doi: 10.1063/1.4949757.

[25] S. Chen, J. Liu, L. Wang, H. Luo, and Y. Gao, "Unraveling mechanism on reducing thermal hysteresis width of VO2 by Ti doping: A joint experimental and theoretical study," *J. Phys. Chem. C*, vol. 118, no. 33, pp. 18938–18944, 2014, doi: 10.1021/jp5056842.

Data Availability

Data for all the figures is available upon reasonable request.

Acknowledgements

MAK acknowledges funding support from ONR N00014-20-1-2297 and NSF 1750341. SR acknowledges funding support from AFOSR grant FA9550-19-1-0351.